



HAL
open science

Charmonium narrow resonances in the string breaking region

J Segovia, D R Entem, F Fernández

► **To cite this version:**

J Segovia, D R Entem, F Fernández. Charmonium narrow resonances in the string breaking region. *Journal of Physics G: Nuclear and Particle Physics*, 2010, 37 (7), pp.75010. 10.1088/0954-3899/37/7/075010 . hal-00630018

HAL Id: hal-00630018

<https://hal.science/hal-00630018>

Submitted on 7 Oct 2011

HAL is a multi-disciplinary open access archive for the deposit and dissemination of scientific research documents, whether they are published or not. The documents may come from teaching and research institutions in France or abroad, or from public or private research centers.

L'archive ouverte pluridisciplinaire **HAL**, est destinée au dépôt et à la diffusion de documents scientifiques de niveau recherche, publiés ou non, émanant des établissements d'enseignement et de recherche français ou étrangers, des laboratoires publics ou privés.

Charmonium narrow resonances in the string breaking region

J. Segovia, D. R. Entem, F. Fernández.

Grupo de Física Nuclear and IUFFyM,

Universidad de Salamanca, E-37008 Salamanca, Spain

Abstract

We study the properties of excited charmonium states near the confinement string breaking region using a screened confinement potential. Recent data on $e^+e^- \rightarrow \Lambda_c \bar{\Lambda}_c$ and $e^+e^- \rightarrow J/\psi \pi \pi$ are discussed. We find that, in this energy region, S and D states became almost degenerated with a narrow width. The measure of these states can contribute to a more accurate knowledge of the confinement interaction.

Keywords: Charmonium, confinement, quark models.

Pacs: 14.40.Gx, 12.39.Pn.

The breaking of the color electric string between two static sources is a phenomenon predicted by QCD and it is the basis of the meson decays and hadronization processes. Although there is no analytical proof, it is a general belief that confinement merge from the force between the gluon color charges. When two quarks are separated, due to the non abelian character of the theory, the gluon fields self interact forming color strings which brings the quarks together. In a pure gluon gauge theory the potential energy of the $q\bar{q}$ pair grows linearly with the quark-antiquark distance. However in full QCD the presence of sea quarks may soften the linear potential, due to the screening of the color charges, and eventually leads to the breaking of the string.

Lattice QCD calculations with dynamical fermions indicate that color screening effects on the linear potential do exist at large distances and can be parametrized in terms of a screening length μ^{-1} [1]. Recently string breaking effects has been shown for $n_f = 2$ lattice QCD [2].

From a phenomenological point of view the screening effects can be related to properties of the quarkonium system. In fact, the knowledge of the highly excited quarkonium states properties may help to determine the form of the confinement in this region.

Very recently [3] the Belle collaboration reported a measurement of the exclusive $e^+e^- \rightarrow \Lambda_c \bar{\Lambda}_c$ cross section. A clear peak at $M = 4634_{-7-8}^{+8+5}$ MeV is observed. Besides this significant near threshold enhancement, the cross section shows several structures up to 5.4 GeV. Similar structures has been observed in the exclusive measurements of the $e^+e^- \rightarrow D^{*\pm} D^{*\mp}$ cross section using initial state radiation [4] and in the analysis of the $e^+e^- \rightarrow J/\psi \pi \pi$ data [5].

These data have been analyzed by different authors. Van Beveren *et al.* [6, 7] conclude that the near threshold enhancement can be explained as a combined effect of a normal threshold behavior and a sub-threshold zero in the amplitude at 4.5 GeV. Moreover, they found indications for four not very broad ($30 \approx 60$ MeV) new $c\bar{c}$ states at 4.79 GeV, 4.87 GeV, 5.13 GeV and 5.29 GeV. On the other hand Bugg [8] concludes from the analysis of the same data that the near threshold enhancement may be interpreted as the $X(4660)$ when a proper form factor is used in the phase space.

Although data are not yet conclusive, the region above the $\Lambda_c \bar{\Lambda}_c$ threshold is of indubitable interest to determine the behavior of the confinement interaction near the string breaking region. In this work we undertake the study of the $J^{PC} = 1^{--} c\bar{c}$ highly excited states which are the accessible quantum numbers from the e^+e^- entrance channel. Our aim is

to characterize these states (energies, leptonic and strong widths, etc) to look for these properties in future experiments. We will use the model of Refs. [9, 10] which describes the hadron spectrum [11] and the hadron-hadron interaction [12]. The model incorporates color screening effect through a confinement potential similar to the one obtained in lattice calculations [1]. This model has been applied to a careful study of the $J^{PC} = 1^{--} c\bar{c}$ sector in Ref. [10]. In this reference most of the new 1^{--} resonances are interpreted as $q\bar{q}$ states. The $X(4360)$ is found to be the $4S$ state and then the $\psi(4415)$ appears as the $3D$ one. This assignment differs from the standard one but agree with the new measurements of its leptonic width [13]. Moreover the $Y(4260)$, now included in PDG as $X(4260)$ [14], does not appear as $q\bar{q}$ pair. This is consistent with the recent measurement of BaBar [15] of the exclusive production of $D\bar{D}$, $D^*\bar{D}$ and $D^*\bar{D}^*$ which did not find evidence for the $X(4260)$ decays in these channels as expected if the $X(4260)$ were a $J^{PC} = 1^{--}$ charmonium state.

Similar calculation has been performed by other authors with rather different conclusions. So Li *et al.* [16], using also a screened potential but with different parametrization, are able to reproduce the $X(4260)$ as a $c\bar{c}$ state but loss the well established $\psi(4160)$ which appears too low in mass. The wide range of theoretical predictions demands more accurate data to constrain the different models.

As stated above our model assumes a confinement potential suggested by lattice calculation with dynamical fermions [1]

$$V_{CON}(\vec{r}_{ij}) = \{-a_c(1 - e^{-\mu_c r_{ij}}) + \Delta\}(\vec{\lambda}_i^c \cdot \vec{\lambda}_j^c) \quad (1)$$

where λ_j^C are the color matrices and Δ is a global constant to fix the energy origin. This constant is flavor independent and is fitted to the all meson spectrum [9]. At short distances the potential presents a linear behavior with an effective confinement strength $a = -a_c\mu_c(\vec{\lambda}_i^C \cdot \vec{\lambda}_j^C)$ while at large distances shows a threshold given by

$$V_{thr} = \{-a_c + \Delta\}(\vec{\lambda}_i^c \cdot \vec{\lambda}_j^c) \quad (2)$$

Li *et al.* [17] have shown that this potential gives similar global features that a coupled channel calculation based on the Cornell potential and therefore describes, in an effective way, the effects of dynamical light quark pair creation.

No $q\bar{q}$ bound states can be found for energies higher than this threshold. Therefore at this scale the system undergo a transition from a color string configuration between two

static sources into a pair of mesons. Obviously the value of V_{thr} is an outcome of our fit and experimental data of highly excited states may help to determine its value and/or the form of the confinement potential in this region in a precise way.

Besides the confinement interaction in the charm sector, quarks and antiquarks interact through one gluon exchange (OGE) [18]

$$\mathcal{L}_{gqq} = i\sqrt{4\pi\alpha_s}\bar{\psi}\gamma_\mu G_c^\mu \lambda^c \psi \quad (3)$$

where λ^c are the $SU(3)$ color matrices and G_c^μ is the gluon field. Expressions for the potentials coming from the non relativistic reduction of OGE are given in Appendix A.

In the light sector quarks also interact through Goldstone boson exchanges coming from the spontaneous breaking of the chiral symmetry [9]. Although in the sector we are going to describe this interaction does not act, it is worth to mention it here because most of the parameters, including those of the confinement interaction, are fitted to the all meson spectrum.

The wide energy range covered by a consistent description of light, strange and heavy mesons requires an effective scale-dependent strong coupling constant that cannot be obtained from the usual one-loop expression of the running coupling constant because it diverges at $Q = \Lambda_{QCD}$. We use the frozen coupling constant of Ref. [9]

$$\alpha_s(\mu) = \frac{\alpha_0}{\ln\left(\frac{\mu^2 + \mu_0^2}{\Lambda_0^2}\right)} \quad (4)$$

where μ is the reduced mass of the $q\bar{q}$ pair and α_0 , μ_0 and Λ_0 are parameters of the model determined by a global fit to the hyperfine splitting from the light to the heavy quark sector. All model parameters are given in Table I.

Meson masses can be found by solving the Schrödinger equation with this interactions using the Gaussian Expansion Method [10].

Masses are not the only observable of the meson system. In fact decay widths allow to check particular regions of the wave function and not an average over the all meson size as in the calculation of the mass spectrum. Thus leptonic decays are sensitive to the meson wave function at the origin and allows to discriminate between S and D states or conventional $c\bar{c}$ states from multiquark systems. Moreover, strong decays give information about the total width of the state and the decay channels which is very usefull for its experimental determination.

quark masses	m_n (MeV)	313
	m_s (MeV)	555
	m_c (MeV)	1763
	m_b (MeV)	5110
Goldstone bosons	m_π (fm ⁻¹)	0.70
	m_σ (fm ⁻¹)	3.42
	m_K (fm ⁻¹)	2.51
	m_η (fm ⁻¹)	2.77
	Λ_π (fm ⁻¹)	4.20
	Λ_σ (fm ⁻¹)	4.20
	Λ_K (fm ⁻¹)	4.21
	Λ_η (fm ⁻¹)	5.20
	$g_{ch}^2/4\pi$	0.54
	θ_p (°)	-15
Confinement	a_c (MeV)	507.4
	μ_c (fm ⁻¹)	0.576
	Δ (MeV)	184.4
	a_s	0.81
OGE	α_0	2.118
	Λ_0 (fm ⁻¹)	0.113
	μ_0 (MeV)	36.98
	\hat{r}_0 (fm)	0.181
	\hat{r}_g (fm)	0.259

TABLE I: Values used for the parameters of the model.

To describe the leptonic width we will use the van Royen-Weisskopf formula [19] modified by QCD radiative corrections [20]

$$\Gamma(n^3S_1 \rightarrow e^+e^-) = \frac{4\alpha^2 e_c^2 |R_n(0)|^2}{M_{nS}^2} \left(1 - \frac{16\alpha_s}{3\pi}\right) \quad (5)$$

$$\Gamma(n^3D_1 \rightarrow e^+e^-) = \frac{25\alpha^2 e_c^2}{2m_c^4 M_{nD}^2} |R_n''(0)|^2. \quad (6)$$

where M_{nS} (M_{nD}) is the mass for the nS (nD) state, $e_c = 2/3$ the quark charge in units of electron charge, α the fine structure constant, $R_{nS}(0)$ the S -wave radial function at the origin and $R_{nD}''(0)$ the second derivative of the D -wave radial function at the origin.

Meson strong decay is a complex non perturbative process that still has not been described from first principles. Instead, phenomenological models has been developed to deal with this problem. We will use the 3P_0 model where the quark-antiquark pair is created from the vacuum. The model was first proposed by Micu [21] and further developed by Le Yaouanc *et al.* [22]. To describe the meson decay process $A \rightarrow B + C$ it assumes that a quark and an antiquark is created with $J^{PC} = 0^{++}$ quantum numbers. The created $q\bar{q}$ pair together with the $q\bar{q}$ pair in the original meson regroupes in the two outgoing mesons via a quark rearrangement process. Then, the transition operator is given by [23]

$$T = -3\gamma \sum_{\mu} \int d^3p d^3p' \delta^{(3)}(p + p') \left[\mathcal{Y}_1 \left(\frac{p - p'}{2} \right) b_{\mu}^{\dagger}(p) d_{\nu}^{\dagger}(p') \right]^{C=1, I=0, S=1, J=0} \quad (7)$$

where μ ($\nu = \bar{\mu}$) are the quark (antiquark) quantum numbers and γ is a dimensionless constant that denotes the strength of the $q\bar{q}$ pair creation from the vacuum.

Defining the S-matrix as

$$\langle f|S|i \rangle = I + i(2\pi)^4 \delta^4(p_f - p_i) \mathcal{M} \quad (8)$$

where \mathcal{M} is the decay amplitude of the process $A \rightarrow B + C$, the decay width in terms of the partial wave amplitude using the relativistic phase space is

$$\Gamma = 2\pi \frac{E_B E_C}{k M_A} \sum_{JL} |\mathcal{M}_{JL}|^2 \quad (9)$$

where k is the on-shell relative momentum of the decaying mesons.

Using the parameters of Table I and equations (5), (6) and (9) we have performed a calculation of the main properties of the excited charmonium states in a screened potential up to the threshold. In Table II we summarize our results. The near threshold enhancement is interpreted as a bound state at $M = 4614$ MeV or $M = 4641$ MeV. In addition we found 14 bound states up to 12^3S_1 and 11^3D_1 . Some of them coincides with the one suggested by [7] although, given the experimental uncertainties, we do not want to stress too much this agreement. The main feature concerning the masses is that as far as we approach to the breaking threshold the S and D states become more and more degenerated making difficult to separate them experimentally. Moreover the leptonic and strong widths become smaller.

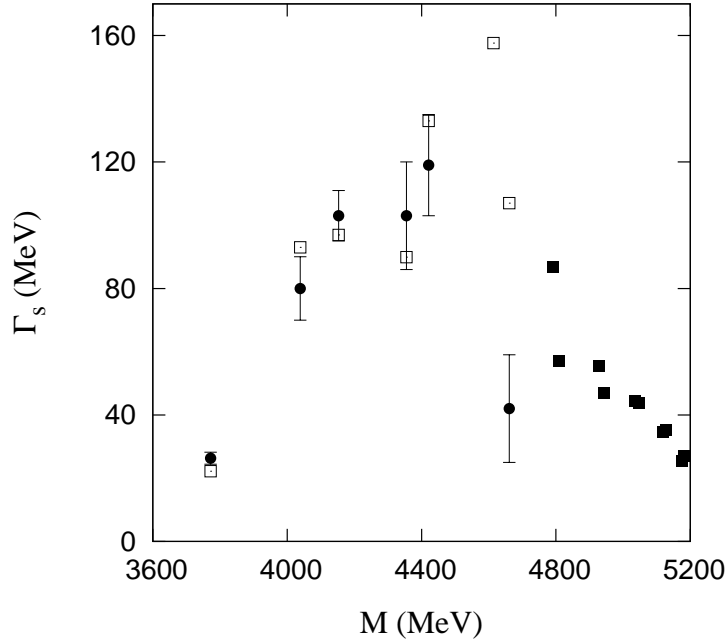


FIG. 1: Total widths for the $c\bar{c} 1^{--}$ states discussed in the text. Solid dots shows the experimental data taken from [14, 24]. Solid (open) squares shows the results of the present (from Ref. [10]) calculation.

This can be seen in Figs. 1 and 2 where, for completeness, we have included the results obtained in Ref. [10] with the same model. The measured strong widths agree reasonably well with our calculation reaching a maximum around a mass of $M = 4600$ MeV. After this maximum, the widths decrease due to the competition between phase space and meson wave function overlaps. In almost all the resonances the most important decay channel is the D^*D^* . The experimental data around 4700 MeV is clearly out of the systematic, which maybe an indication of a more complex structure of the 4660 state.

The situation is similar regarding the leptonic widths shown in Fig. 2. As in the former figure we show the results of Ref. [10] for the lower masses together with our current results. Once again the model reproduces the measured widths showing a clear difference between S and D wave states. This behavior is an important tool to assign quantum numbers to the resonances. In particular the measure of the $X(4360)$ leptonic width will confirm the assignment given in Ref. [10]. As far as we are approaching to the threshold the widths are narrower and the difference between S and D states become smaller.

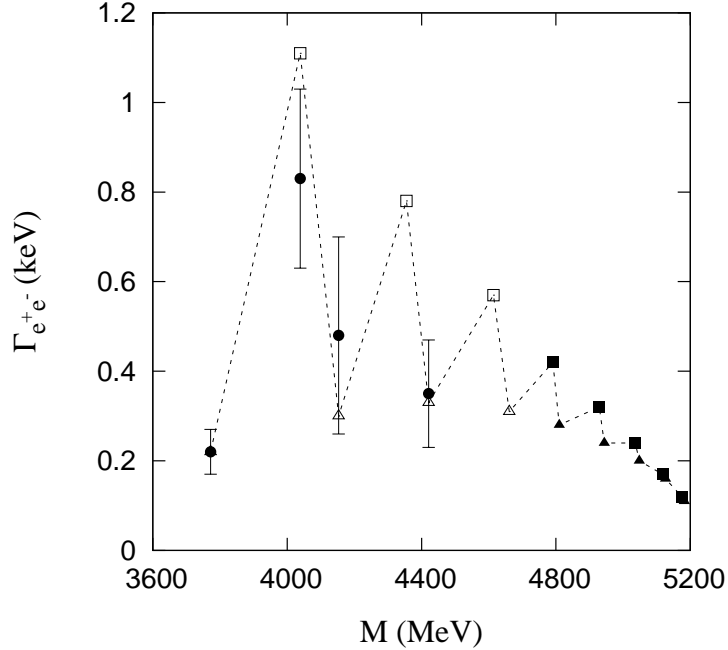


FIG. 2: Leptonic widths for the $c\bar{c} 1^{--}$ states discussed in the text. Solid dots shows the experimental data taken from [13, 14]. Solid (open) squares shows the results for S -wave states for the present (from Ref. [10]) calculation. The same is represented with triangles for D -wave states.

In Fig. 3 we show the quadratic mean radius for these mesons. As expected these are extended objects with a radius that grows as one gets closer to the threshold.

Then the scenario drawn from this calculation consists in several narrow resonances near the breaking threshold which include S and D -wave states. The only possible way to resolve these two angular momentum contributions is to look to some specific ratio, like $R = \frac{X \rightarrow DD^*}{X \rightarrow D^*D^*}$ shown in Fig. 4, which range from 1.5 to 0.7 for S -wave states and is around 0.2 for D states.

Finally we compare our results with the $e^+e^- \rightarrow J/\psi\pi\pi$ and $e^+e^- \rightarrow \Lambda_c\bar{\Lambda}_c$ data. We will use those of van Beveren *et al.* [6, 7] where the subtraction of the non-resonant signal has been carried out assuming Breit Wigner forms for the $c\bar{c}$ resonances. Some of the experimental predicted structures are well reproduced. The most significant differences are the resonance below 4900 MeV and the one around 5300 MeV. The discrepancy at 4900 MeV can not be explained by interference effects or modifications in the Breit-Wigner shapes because the nearby resonances are too separated, as shown in Fig. 5. The discrepancy around 5300 has a different origin because our threshold is below this region.

State	$M_{QM}(\text{MeV})$	$M_{exp}(\text{MeV})$	$\Gamma_{e^+e^-}(\text{keV})$	Dominant	\mathcal{BR}	$\Gamma_T(\text{MeV})$
5^3S_1	4614		0.57	$D^*D_2^*$	0.41	164.6
4^3D_1	4641	4664 ± 11	0.31	D^*D^*	0.30	107.5
6^3S_1	4791	4790	0.42	$D^*D_2^*$	0.33	86.9
5^3D_1	4810		0.28	D^*D^*	0.40	57.0
		4870				
7^3S_1	4929		0.32	D^*D^*	0.20	55.6
6^3D_1	4944		0.24	D^*D^*	0.40	46.8
8^3S_1	5036		0.24	D^*D^*	0.24	44.3
7^3D_1	5048		0.20	D^*D^*	0.33	43.8
9^3S_1	5117		0.17	D^*D^*	0.26	34.5
8^3D_1	5126	5130	0.16	D^*D^*	0.30	35.3
10^3S_1	5175		0.12	D^*D^*	0.25	25.3
9^3D_1	5182		0.11	D^*D^*	0.27	27.1
11^3S_1	5214		0.07	D^*D^*	0.24	16.91
10^3D_1	5219		0.07	D^*D^*	0.25	17.81
12^3S_1	5236		0.03	D^*D^*	0.24	8.49
11^3D_1	5239		0.03	D^*D^*	0.24	8.35
		5290				

TABLE II: High excited states of $c\bar{c}$ with quantum numbers $J^{PC} = 1^{--}$.

In order to show the sensitivity of the spectra to the confinement potential parameters we have change a_c and μ_c in Eq.(1), leaving its product constant, which guarantees that the slope of the confinement remains the same. The results are shown in Fig. 6. With this parametrization we clearly improve the agreement in the 5300 MeV region, although the precision of the data is not enough to decide about the 4900 MeV region. The price to pay is to loose part of the consistency with the whole meson spectra. These results show the interest of this region to constrain the confinement interaction.

As a summary, we have studied the properties of the $c\bar{c}$ resonances near the string breaking threshold using a screened confinement potential. These states show narrow leptonic and

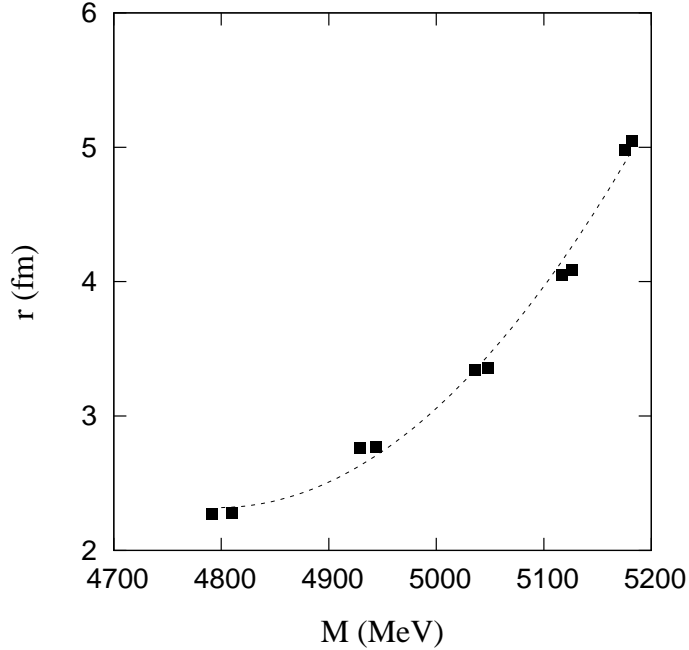


FIG. 3: Solid square shows the theoretical mean square radius of the resonances in Table II.

strong widths and are very extended objects. They show a promising agreement with the scarce experimental data, although more experimental and theoretical work is needed in this interesting region to gain more insight into the properties of confinement.

APPENDIX A: THE QUARK-QUARK POTENTIAL

In this appendix we give explicit expressions for the different pieces of the quark-quark potential. They contain central, tensor and spin-orbit terms that will be grouped for consistency.

1. Gluon exchange interaction

The central part of the OGE reads

$$V_{OGE}^C(\vec{r}_{ij}) = \frac{1}{4}\alpha_s(\vec{\lambda}_i^c \cdot \vec{\lambda}_j^c) \left[\frac{1}{r_{ij}} - \frac{1}{6m_i m_j} (\vec{\sigma}_i \cdot \vec{\sigma}_j) \frac{e^{-r_{ij}/r_0(\mu)}}{r_{ij} r_0^2(\mu)} \right] \quad (\text{A1})$$

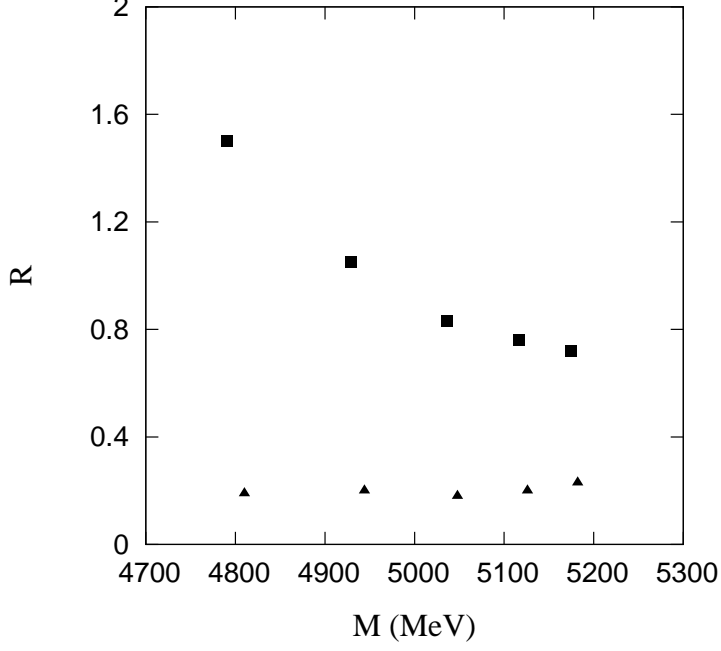


FIG. 4: The ratio $R = \frac{X \rightarrow DD^*}{X \rightarrow D^* D^*}$ predicted by the model is shown by solid squares (triangles) for S -wave (D -wave) states.

where the delta function is regularized as

$$\delta(r_{ij}) \rightarrow \frac{1}{4\pi} \frac{e^{-r_{ij}/r_0(\mu)}}{r_{ij} r_0^2(\mu)} \quad (\text{A2})$$

with $r_0(\mu) = \hat{r}_0 \frac{\mu_{nn}}{\mu_{ij}}$ scales with the reduced mass as expected for a Coulombic system.

The noncentral potentials, tensor and spin-orbit, have the form

$$V_{OGE}^T(\vec{r}_{ij}) = -\frac{1}{16} \frac{\alpha_s}{m_i m_j} (\vec{\lambda}_i^c \cdot \vec{\lambda}_j^c) \left[\frac{1}{r_{ij}^3} - \frac{e^{-r_{ij}/r_g(\mu)}}{r_{ij}} \left(\frac{1}{r_{ij}^2} + \frac{1}{3r_g^2(\mu)} + \frac{1}{r_{ij} r_g(\mu)} \right) \right] S_{ij} \quad (\text{A3})$$

$$V_{OGE}^{SO}(\vec{r}_{ij}) = -\frac{1}{16} \frac{\alpha_s}{m_i^2 m_j^2} (\vec{\lambda}_i^c \cdot \vec{\lambda}_j^c) \left[\frac{1}{r_{ij}^3} - \frac{e^{-r_{ij}/r_g(\mu)}}{r_{ij}^3} \left(1 + \frac{r_{ij}}{r_g(\mu)} \right) \right] \\ \times \left[((m_i + m_j)^2 + 2m_i m_j) (\vec{S}_+ \cdot \vec{L}) + (m_j^2 - m_i^2) (\vec{S}_- \cdot \vec{L}) \right] \quad (\text{A4})$$

where $\vec{S}_\pm = \vec{S}_i \pm \vec{S}_j$ and $r_g(\mu) = \hat{r}_g \frac{\mu_{nn}}{\mu_{ij}}$ scales as the central term. Finally we use an effective scale dependent strong coupling constant given by Eq. (4).

2. Confinement

The screened confinement potential is written as

$$V_{CON}^C(\vec{r}_{ij}) = \left[-a_c(1 - e^{-\mu_c r_{ij}}) + \Delta \right] (\vec{\lambda}_i^c \cdot \vec{\lambda}_j^c). \quad (\text{A5})$$

The spin-orbit contribution is a combination of scalar and vector terms

$$V_{CON}^{SO}(\vec{r}_{ij}) = (\vec{\lambda}_i^c \cdot \vec{\lambda}_j^c) \frac{a_c \mu_c e^{-\mu_c r_{ij}}}{4m_i^2 m_j^2 r_{ij}} \left[((m_i^2 + m_j^2)(1 - 2a_s) + 4m_i m_j (1 - a_s)) (\vec{S}_+ \cdot \vec{L}) + (m_j^2 - m_i^2)(1 - 2a_s) (\vec{S}_- \cdot \vec{L}) \right] \quad (\text{A6})$$

where a_s controls the ratio between them.

-
- [1] Born K D *et al* 1989 *Phys. Rev. D* **40** 1653
 - [2] Bali G S *et al* (SESAM Collaboration) 2005 *Phys. Rev. D* **71** 114513
 - [3] Pakhlova G *et al* (Belle Collaboration) 2008 *Phys. Rev. Lett.* **101** 172001
 - [4] Pakhlova G *et al* (Belle Collaboration) 2007 *Phys. Rev. Lett.* **98** 092001
 - [5] Aubert B *et al* (BaBar Collaboration) 2005 *Phys. Rev. Lett.* **95** 142001
 - [6] van Beveren E and Rupp G 2009 arXiv:0904.4351
 - [7] van Beveren E, Liu X, Coimbra R and Rupp G 2009 *Europhys. Lett.* **85** 61002
 - [8] Bugg D V 2009 *J. Phys. G* **36** 075002
 - [9] Vijande J, Fernández F and Valcarce A 2005 *J. Phys. G* **31** 481
 - [10] Segovia J, Yasser A M, Entem D R and Fernández F 2008 *Phys. Rev. D* **78** 114033
 - [11] Garcilazo H, Valcarce A and Fernández F 2001 *Phys. Rev. C* **63** 035207. Vijande J, Garcilazo H, Valcarce A and Fernández F 2004 *Phys. Rev. D* **70** 054022.
 - [12] Fernández F, Valcarce A, Gonzalez P and Vento V 1992, *Phys. Lett. B* **287** 35.
 - [13] Ablikim M *et al* (BES Collaboration) 2008 *Phys. Lett. B* **660** 315.
 - [14] Amsler C *et al* (Particle Data Group) 2008 *Phys. Lett. B* **667** 1
 - [15] B Aubert *et al* (BaBar Collaboration) 2009 *Phys. Rev. D* **79** 092001
 - [16] Li B Q and Chao K T 2009 *Phys. Rev. D* **79** 094004
 - [17] Li B Q, Meng C and Chao K T 2009 *Phys. Rev. D* **80** 014012
 - [18] De Rjula A, Georgi H and Glashow S L 1975 *Phys. Rev. D* **12** 147

- [19] Van Royen R and Weisskopf V F 1967 *Nuovo Cim.* **50** 617; **51** 583
- [20] Barbieri R, Gatto R, Kögerler R and Kunszt Z 1975 *Phys. Lett.* **57B** 455; Kwong W, Mackenzie P B, Rosenfeld R and Rosner J L 1988 *Phys. Rev. D* **37** 3210
- [21] Micu L 1969 *Nucl. Phys. B* **10** 521
- [22] Le Yaouanc A, Oliver L, Pene O and Raynal J-C 1973 *Phys. Rev. D* **8** 2223
- [23] Bonnaz R and Silvestre-Brac B 1999 *Few-Body Syst.* **27** 163
- [24] Liu Z Q, Qin X S and Yuan C Z 2008 *Phys. Rev. D* **78** 014032

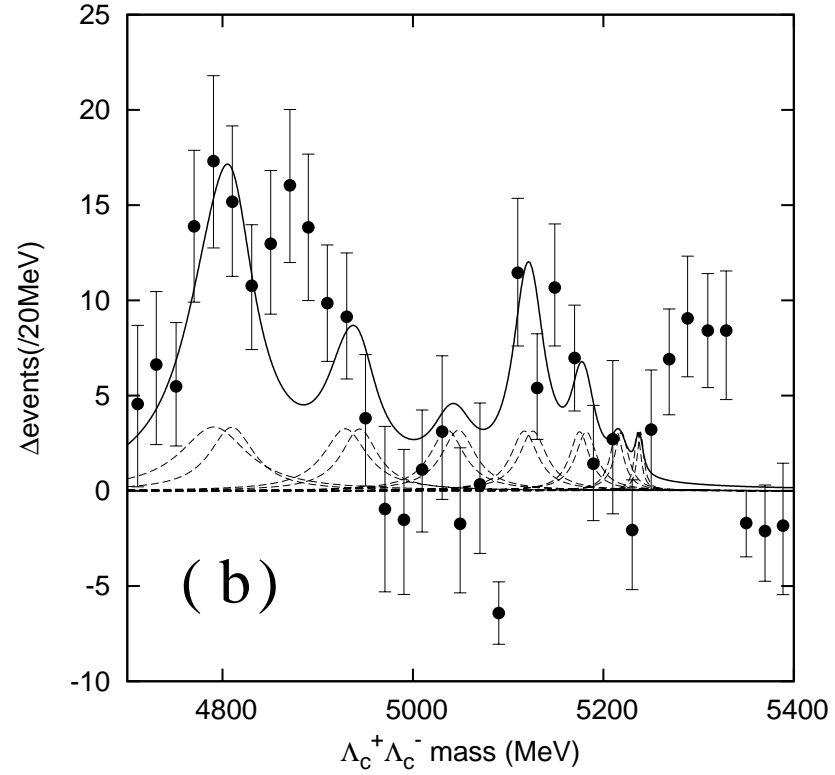
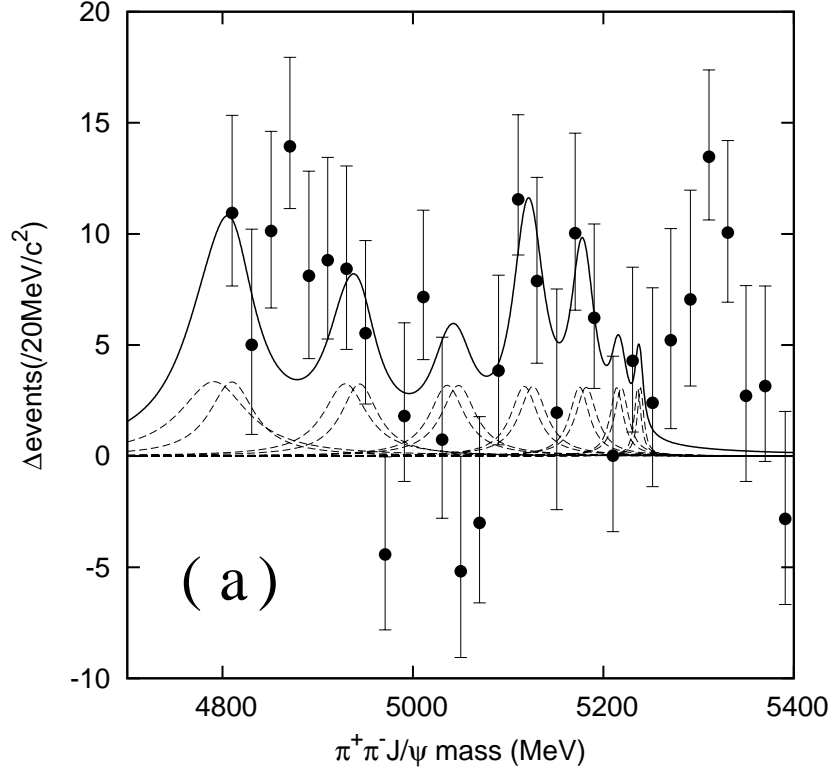


FIG. 5: Fit to $J/\Psi\pi^+\pi^-$ [6] and the $e^+e^- \rightarrow \Lambda_c^+\Lambda_c^-$ [7] data, shown by solid dots, using the resonances from Table II. The solid line shows the full result while the dashed lines show the position of each resonance.

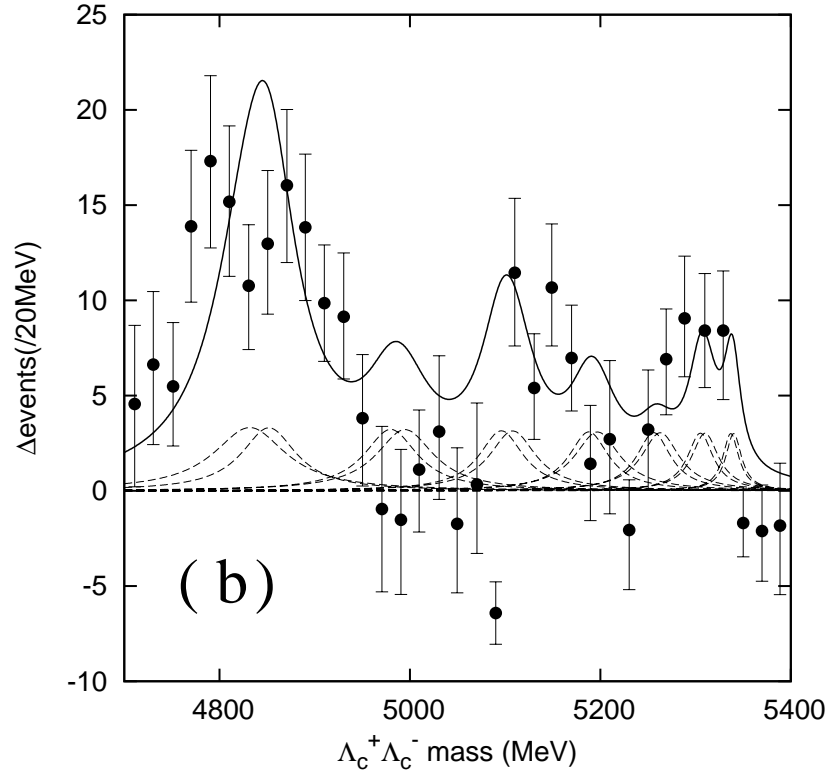
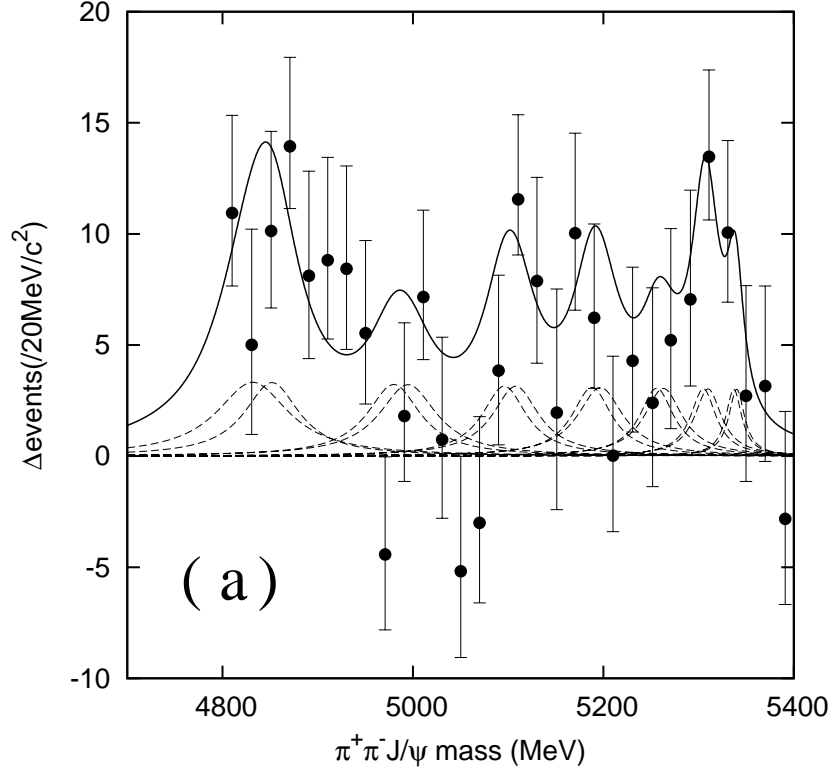


FIG. 6: Same as in Fig. 5 varying the confinement parameters as explained in the text.